

Mechanical properties and corrosion resistance of low-alloy steels in atmospheric conditions containing chloride

Y.Y. Chen^a, H.J. Tzeng^b, L.I. Wei^b, H.C. Shih^{a,*}

^a Department of Materials Science and Engineering, National Tsing Hua University, 101, Sec. 2, Kuang Fu Road, Hsinchu 300, Taiwan ROC

^b China Steel Corporation, 1 Chung-Kang Road, Kaohsiung 812, Taiwan ROC

Received 27 September 2004; received in revised form 9 February 2005; accepted 17 February 2005

Abstract

The corrosion resistance (weight loss) and mechanical properties (i.e., yield strength, ultimate tensile strength, and elongation) of four newly developed low-alloy steels (LAS) were compared with a weathering steel (Acr-Ten A) and a carbon steel (SS400) using a laboratory-accelerated test that involved cyclic wet/dry conditions in a chloride environment (5 wt.% NaCl). The new LAS were designated 1604A, 1604B, 1605A, and 1605B. After 72 cycles of cyclic corrosion tests, the change in mechanical properties by corrosion was the least for SS400, Acr-Ten A was second, and effects of corrosion on the mechanical properties of the other four low-alloy steels were similar. The susceptibility of the steels to corrosion based on their weight loss was the most for SS400, and the least for 1605A and 1605B. In addition, it was found that the corrosion potentials of low-alloy steels are more active prior to accelerated corrosion tests than after the accelerated test, and the corrosion tendency of the six steels immersed in 3.5 wt.% NaCl solutions after 72 cycles of accelerated corrosion tests was the least for 1605A and 1605B because the corrosion potentials were higher than other steels. The rust characteristics observed by SEM and analyzed by FTIR and EPMA indicated that most of the rust layers on the test steels were composed of a loose outer rust layer and a dense inner rust layer. The outer rust layer of each steel was composed of α -FeOOH, γ -FeOOH, magnetite (Fe_3O_4), H_2O , and amorphous ferric oxyhydroxide ($\text{FeO}_x(\text{OH})_{3-2x}$, $x=0$ to 1), while the inner rust layer was composed mainly of Fe_3O_4 with a little α -FeOOH. In addition, it was apparent that the copper and chromium alloying additions were enriched, respectively, at the rust-layer/substrate interface and in the rust layers. Finally, combining the results of the accelerated tests, the rust layer analysis, and the corrosion potential measurements showed that low-alloy steels, such as 1605A and 1605B, have better weathering steel properties than Acr-Ten A for use in the humid and salty weather.

© 2005 Elsevier B.V. All rights reserved.

Keywords: Atmospheric corrosion; Weathering steel; Accelerated test; Weight loss; Rust layer; Corrosion potential

1. Introduction

Atmospheric corrosion is a relatively complex process, involving a metal/electrolyte interface, corrosion products, and chemical environments. It is generally an electrochemical process in the presence of a thin layer of electrolyte on the surface of the metal. The electrolyte carries various chemicals precipitated from the atmosphere, and is of decisive importance for the atmospheric corrosion. When evaluating the corrosion behavior of metals in different test locations, consideration of the composition of atmospheric deposits is

very important. For example, in coastal environments, the atmospheres mainly contain chloride, while in industrial environments, SO_2 predominates. However, it is well known that except for stainless steels, which are more costly, almost no uncoated or unalloyed steels can resist the influences of various corrosion factors coming from the atmosphere (e.g., sulfide, chloride, dust, and moisture) for long periods of exposure. Weathering steel (WS) is a kind of steel that can be maintained for dozens of years at low cost and without coating. The enhanced corrosion resistance of weathering steels is attributed to the formation of a tightly adherent protective rust layer, which has been shown to be related both to the alloying elements and to the environmental conditions under which the rust formed [1–7]. Due to its numerous advan-

* Corresponding author. Tel.: +886 3 5715131x3845; fax: +886 3 5710290.
E-mail address: hcshih@mse.nthu.edu.tw (H.C. Shih).

tages, WS has potential application in the civil engineering and automobile industries. For example, they are employed in the construction of buildings and bridges and for architectural trim without the necessity of painting, thereby saving appreciable maintenance costs over the life of the structure. Therefore, it makes sense to tailor WS alloys for specific environments and substitute them for the less corrosion-resistant common steels wherever applicable.

The development of weathering steels dates back to the 1930s and they have been used widely since then because of their unique corrosion resistance [8,9]. In the 1950s, a WS called Cor-Ten A [8–11] was developed in North America. Its outstanding corrosion resistance is suitable for the North American continental climate, but it does not perform as well in the semi-tropical monsoon climate of an island with high humidity and salinity. The seasonal monsoons bring large amounts of sea salt, and even the higher levels of air pollution can contribute to more aggressive conditions for corrosion. For this reason, it is necessary to develop different types of WS that are suitable locally. Therefore, the high phosphorus weathering steel, the so-called Acr-Ten A, has been demonstrated to have a better corrosion resistance than carbon steels (CS) in various atmospheres of Taiwan island [12,13].

Misawa et al. [14] and Yamashita et al. [15] investigated the growth of the protective rust layer formed on weathering steel in a marine atmosphere, and found that the protective layer on traditional weathering steel could not form because of the corrosion by the chloride ions. However, in industrial and rural atmospheres, the rust layer formed readily on weathering steel, which acted as a barrier to slow down the corrosion process [9,14]. Furthermore, Okada et al. [1] pointed out that the protective rust layer on weathering steel was actually composed of two layers: the inner rust layer, enriched with alloying elements like Cr, Cu, and others, was compact and had a protective ability, whereas the outer layer, containing cracks and pores, could not inhibit the entrance of the corrosive electrolyte.

Studies on atmospheric corrosion are traditionally carried out by field exposure tests. Since natural exposure tests are by their very nature relatively long, it is necessary to assess the durability of materials used in certain environments by accelerated laboratory experiments [7]. In principle, atmospheric corrosion is primarily ascribed to electrochemical processes occurring on a metallic surface under wet/dry conditions. Consequently, it is likely that most, if not all, corrosion results from the liquid-phase reactions [16]. Cyclic wet/dry conditions and Cl^- concentration are important controlling parameters in accelerated tests. According to numerous studies using accelerated tests [6,7,14,17,18], the rust layers formed on WS are less protective than those on carbon steel (CS) under continuously wet conditions such as when they are buried in soil or totally immersed in water; however, the intermittent wet/dry process facilitates the formation of a protective rust layer on WS that enhances its corrosion resistance. Therefore, a cyclic salt spray and ultraviolet light-

ing are used to simulate the intermittent wet/dry corrosion environment in chloride-containing atmospheres. Also, the difference between the mechanical and the electrochemical properties before and after the accelerated tests are frequently measured.

Generally speaking, the corrosion products on the surface of WS are mainly α -FeOOH, γ -FeOOH, β -FeOOH, $\text{Fe}(\text{OH})_3$, and Fe_3O_4 . These products can coexist partly as crystalline and partly as amorphous structures [6,14]. When the steel contacts moisture and corrodes, the initial corrosion product is mainly γ -FeOOH, but gradually this transforms to α -FeOOH as a result of the intermittently wet/dry conditions [6,14]. The alloying additions in WS result in corrosion products that are denser and more stable than those on CS. Although α -FeOOH and γ -FeOOH can also be observed in corrosion products on CS, they are porous in nature since they are not enhanced by the alloying elements, and, in addition, the adhesion is poor between the rust layer and the substrate. Consequently, the corrosive species can readily penetrate the porous rust layers to the substrate where corrosion reactions may proceed endlessly. It is apparent that the rust layers on CS provide little or no protection to the substrate.

In this study, we compared the atmospheric corrosion resistance (weathering resistance) of the four low-alloy steels (LAS) that were developed by China Steel Corp., with two other alloys (Acr-Ten A and SS400) to identify the alloying elements that confer additional corrosion resistance and/or mechanical strength. We also investigated the change in mechanical properties and corrosion potentials before and after these accelerated tests. Finally, we analyzed the morphology, bonding nature, and chemistry of the rust products using SEM, FTIR, and EPMA, respectively.

2. Experimental procedures

2.1. Test materials

Four LASs, designated 1604A, 1604B, 1605A, and 1605B, were compared with the commercial high-phosphorus WS (Acr-Ten A) and with CS (SS400). The chemical compositions (wt.%) were analyzed by an inductively coupled plasma-atomic emission spectrometer (ICP-AES) and are listed in Table 1. The coiling temperature of 1605B was 400 °C, but the other three steels were coiled at 600 °C. The test materials were all cut into reduced plate tensile specimens, 6.25 mm in width, for the accelerated laboratory tests according to ASTM E 8M-98 [19]; specimen dimensions are shown in Fig. 1. Fig. 2(a)–(f) show the surface microstructures of the five as-received LASs (1604A, 1604B, 1605A, 1605B, and Acr-Ten A) and the CS (SS400). They were all first mechanically wet ground using a 1200 grit SiC paper and then etched in a Nital solution (98% nitric acid + 2% alcohol) for ~25s. The microstructures of 1604A (Fig. 2(a)), and 1604B (Fig. 2(b)), as shown by SEM, are both

Table 1
Chemical compositions of the test materials (wt.%)

Steel	Fe	C	Si	Mn	P	S	Cu	Ni	Cr	Al	N	Ti
1604A	Bal.	0.01	0.008	1.19	0.06	0.008	0.31	0.16	–	0.033	0.0028	0.023
1604B	Bal.	0.011	0.008	1.19	0.091	0.008	0.30	0.16	–	0.029	0.0028	0.026
1605A	Bal.	0.091	1.06	1.20	0.092	0.0075	0.30	0.16	0.56	0.030	0.0062	–
1605B	Bal.	0.091	1.05	1.20	0.091	0.0075	0.30	0.16	0.56	0.030	0.0062	–
Acr-Ten A	Bal.	0.10	0.44	0.47	0.10	0.008	0.31	0.30	0.55	0.020	–	–
SS400	Bal.	0.13	0.19	0.81	0.015	0.008	0.063	0.049	0.021	0.024	–	–

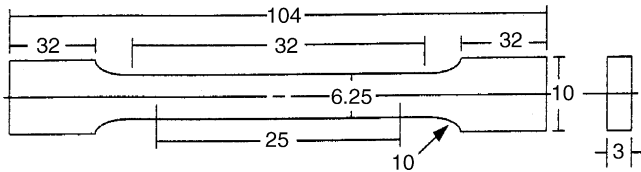


Fig. 1. Schematic drawings of the test specimen machined according to ASTM E8M; dimensions are in mm.

of pure ferrite; 1605A (Fig. 2(c)), Acr-Ten A (Fig. 2(e)), and SS400 (Fig. 2(f)), are all duplex structures consisting of ferrite and small amounts of pearlite; and 1605B (Fig. 2(d)) is composed of ferrite and bainite.

2.2. Alternating wet/dry accelerated corrosion tests

Prior to the accelerated cyclic corrosion tests, all the surfaces of the tensile specimens were polished using 800-grade emery paper, cleaned ultrasonically in acetone, and then rinsed with distilled water before drying in air. All specimens were put simultaneously into the salt spray tester (Q.U.V. Accelerated Weathering Tester) and were mounted at 30° to the horizontal according to the ASTM G 50–76 specification for simulating natural atmospheric corrosion [20]. The accelerated corrosion testing procedure involved cycling between a dry environment and a mist composed of 5 wt.% (~0.86M) NaCl, according to ASTM B 117–97 [21]. Each

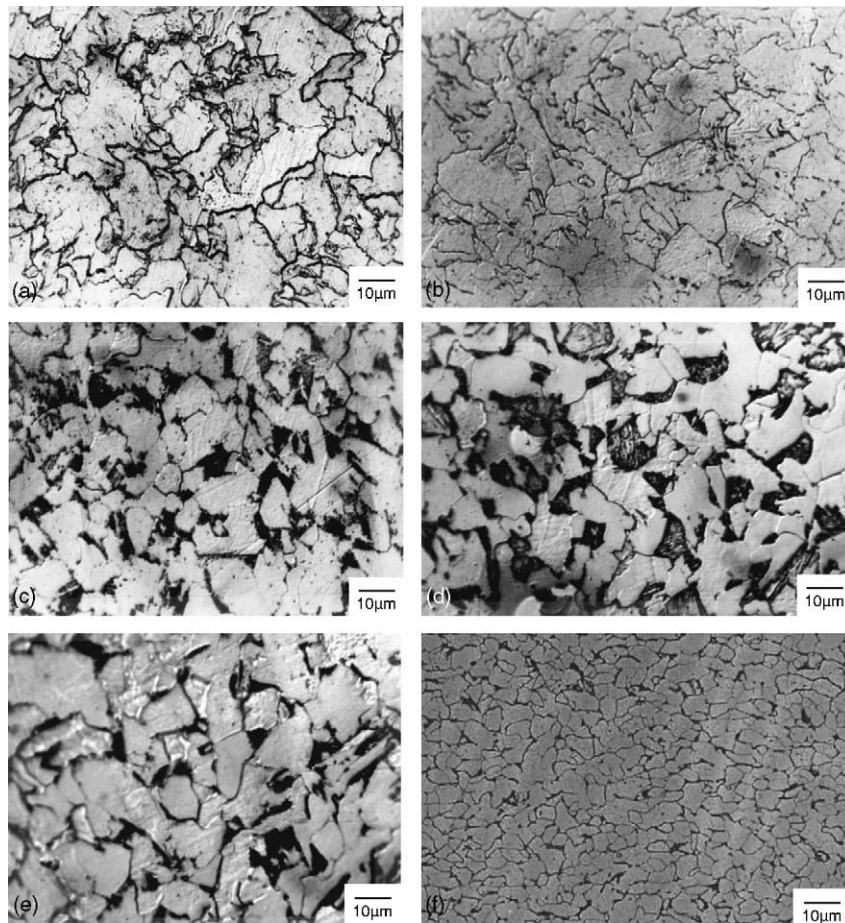


Fig. 2. Surface microstructures of the as-received low-alloy steels and the carbon steel under the scanning electron microscope at a magnification of 1000×: (a) 1604A, (b) 1604B, (c) 1605A, (d) 1605B, (e) Acr-Ten A and (f) SS400.

wet/dry cycle (24 h) consisted of a wetting period (8 h at 35 °C, 97 ± 1% RH) plus a drying period (16 h at 60 °C, 20% RH). The lighting source was an UVB-313 tube. The dry/wet ratio was 2:1, which was more severe than conditions in a previous study (drying period for 18 h and wetting period for 6 h) [13]. This was done to determine whether the differences between WS and CS would be more significant than those under the dry/wet ratio of 3:1 if the time of wetness increased during the 24 h cycle. On the other hand, the chamber temperature during the drying period was raised from 50 °C [13] to 60 °C in order to increase the density of the rust layers [22]. NaCl was provided only during the wetting period, and the NaCl concentration in the chamber was controlled to 5 wt.%. The accelerated corrosion tests lasted for a total of 72 cycles.

2.3. Mechanical properties and weight loss measurements

After a pre-determined numbers of corrosion test cycles (e.g., 18 and 45), the tensile specimens were taken out and pulled to failure in a tensile testing machine (Material Testing System 810). The strain rate was set at 0.1 mm/s. The load and elongation were measured continuously by a load cell and electric dial gauge, respectively, the outputs of which were recorded on a computer-controlled X–Y recorder (YEW MODEL 3025) until fracture occurred. The stress–strain curves were used to determine the yield strength (YS), the ultimate tensile strength (UTS), and the elongation (%). The results were then plotted versus the number of corrosion cycles to compare the steels tested.

In preparation for weight loss measurements after the specimens fractured, corrosion products on the specimen surfaces were removed chemically by immersion in a Clark's solution (100 ml HCl, sp gr 1.19 + 20 g Sb₂O₃ + 50 g SnCl₂) [23] that was vigorously stirred for ~10 min at 25 °C. After corrosion products had been completely removed, the specimens were rinsed with distilled water, dried in air, and then weighed to determine their mass loss.

2.4. Corrosion potential measurements

The electrochemical open-circuit potentials, i.e. corrosion potentials, of the six steels changed from the time before (i.e., 0 cycle) to the time after (72 cycles) the dry/wet accelerated tests. The potentials were measured with a potentiostat/galvanostat (EG&G Princeton Applied Research (PAR) Model 273) using a saturated calomel electrode (SCE) as the reference electrode. The test solution of 3.5 wt.% NaCl was prepared from reagent grade sodium chloride (Merck) and deionized water in equilibrium with the atmosphere. The measurement lasted for 12 h. All electrochemical experiments were carried out at room temperature (~25 °C).

2.5. Rust products, observation and analysis

Throughout the accelerated corrosion tests, the specimens were examined without stripping the rust from the surface. The surface and cross-section of the rust layers were analyzed using various analytical techniques, including scanning electron microscopy (SEM), Fourier transform infrared spectroscopy (FTIR) and electro probe microanalysis (EPMA). Special care was taken to analyze the interface between the steel substrate and its rust layer, and to understand the distribution of the alloying elements at this interface.

3. Results and discussion

3.1. Weight loss

Almost all of the rust layers fell off the tensile specimens as they were being pulled to failure by the MTS 810. The remaining rust was removed by immersing the specimens into the Clark's solution and vigorously stirring. The rust-free specimens were then weighed. The results of the relation between weight loss and the test cycles are listed in Fig. 3. The weight loss data in this study are expressed as the weight loss per unit surface area. In general, the final weight losses are the lowest for 1605A and 1605B, and the highest for SS400. Therefore, the alloys can be arranged in order of decreasing weight loss, as follows: SS400 (pearlite/ferrite) > Acr-Ten A (pearlite/ferrite) > 1604B (ferrite) ≥ 1604A (ferrite) > 1605B (bainite/ferrite) ≥ 1605A (pearlite/ferrite). It is found that the corrosion resistance of steels containing higher chromium and silicon, such as 1605A and 1605B, need a longer time (>30 cycles) to reveal their corrosion resistance. In other words, the corrosion rate of 1605A and 1605B in accelerated tests decreased markedly after ~30 cycles. This means that,

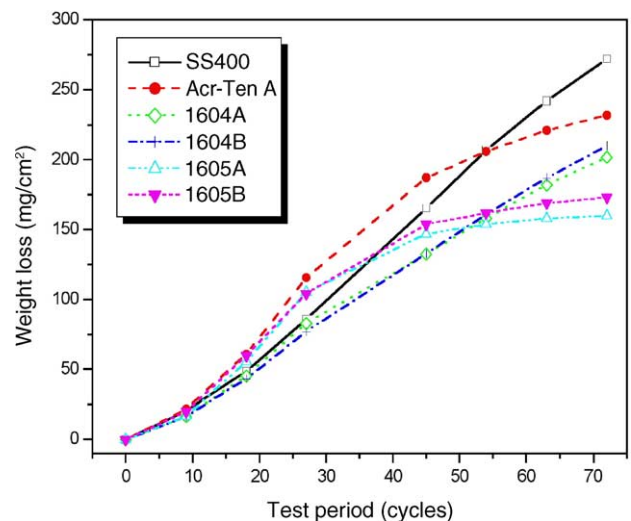


Fig. 3. Relations between the weight loss (mg/cm²) of the steel samples and the test cycles of accelerated cyclic corrosion in a chloride (5 wt.%) environment.

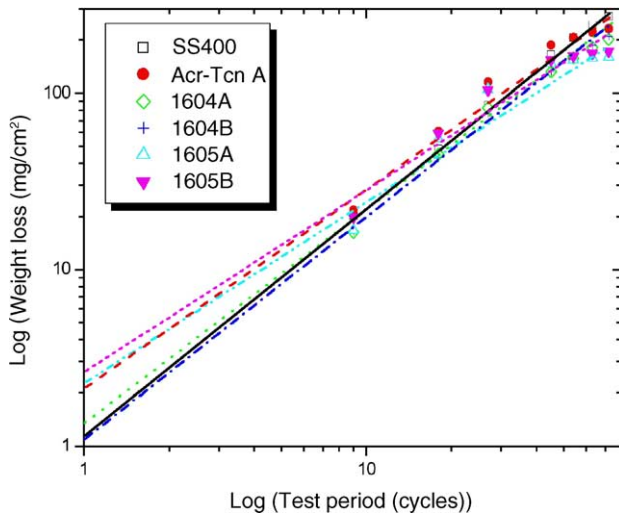


Fig. 4. Bi-logarithmic plots of data points (weight loss vs. test cycles) from Fig. 3.

under these severe cyclic wet/dry test conditions, a longer time is necessary to form adhesive dense rust layers on high-chromium steels, e.g., 1605A, 1605B. A similar phenomenon was observed for Acr-Ten A, but its weathering resistance was less significant than 1605A and 1605B under this environment. On the other hand, for 1604A and 1604B (without Cr), the corrosion rates did not decrease with time. This may be explained by the fact that the dense inner-rust layer did not appear to adhere tightly to the substrate. The adhesion of rust layers will be discussed later. The lowest weight loss occurred in 1604A and 1604B at earlier stages of accelerated corrosion (e.g., <50 cycles) is probably because of their pure ferrite microstructure associated with their low carbon content [7,17]. Finally, the corrosion (weight loss) rate of the common carbon steel (SS400) containing low chromium did not decrease with an increase in the number of test cycles.

The results in Fig. 3 have been re-plotted in Fig. 4 using log–log (bi-logarithm) coordinates to reveal a linear relationship between log (weight loss) and log (test cycles) [13]. Atmospheric corrosion of WS and CS in the accelerated test followed the well-known bi-logarithmic equation:

$$\text{Log } W = \text{Log } X + Y \text{Log } t \quad \text{or} \quad W = X \times t^Y \quad (1)$$

where W is the weight loss (mg/cm^2), t is the exposure time (test cycles), and X and Y are constants. Since X is equal to W when time is unity ($t = 1$), X is considered a measure of the initial corrosion resistance of the metal. On the other hand, Y reflects the change of weight loss with exposure time. Table 2 gives values of the constants in Eq. (1). From Table 2, it can

be seen that the Y values for 1605A (1.0636) and for 1605B (1.0239) are roughly consistent with the previous observations that the corrosion (weight loss) rates for both LASs decrease as time increases. For neutral atmospheric corrosion, the value of Y should not exceed 1. However, it is apparent that the Y values here are >1 . The constant Y approaches 0.5 when an ideal diffusion process is the controlling mechanism. Y values >0.5 result from an acceleration of the diffusion process when the rust is detached by cracking, erosion, dissolution, etc. Conversely, Y values <0.5 arise from a decrease in the diffusion coefficient as the rust layer becomes more and more compact with time. The reason for Y actually being >1 may be that the ratio of wet period/dry period is not optimum. The drying period (16 h) is only twice as long as the wetting period (8 h), and a longer drying time may be necessary to allow for the moist and salty rust layers to become completely dry. In addition, it is possible that the weight loss increases with an increase in the number of test cycles because the presence of thicker rust layers will make it more difficult to dry the surface of the steel. Table 2 shows the X and Y coefficients for the six steels. Also, the difference between the results shown in Fig. 3 and Table 2 for 1605A and 1605B can be explained by the fact that, for a greater number of test cycles, the protective effect of tightly adhesive rust layers outweighs the negative effect of the rust layers absorbing water. Furthermore, the weathering effect becomes more significant as the number of cycle increases.

The values of X and Y obtained from actual exposure tests in the atmosphere can be used to predict the atmospheric corrosion behavior over a longer period of time [24,25]. However, there are still some differences between actual atmospheric exposure and the laboratory simulation test. In an accelerated corrosion test, the environmental variables are more restricted than those of the actual atmosphere in a real life situation. X and Y values are mainly influenced by the chloride concentration, temperature, and the wet/dry period ratio in a salt spray test.

3.2. Effects of corrosion on the mechanical properties

The mechanical properties of the as-received LASs are listed in Table 3. These data were used as a standard against which mechanical properties obtained after the accelerated corrosion tests could be compared.

After the accelerated cyclic corrosion testing, all the tensile specimens were pulled to failure in a MTS 810 machine to measure their mechanical properties. Figs. 5 and 6 show that the mechanical strength (Y_S and UTS) of the steels decreases with an increase in the number of test cycles. The

Table 2
Linear regression coefficients of Eq. (1) for the steel samples after the cyclic accelerated corrosion tests

Coefficient\steels	SS400	Acr-Ten A	1604A	1604B	1605A	1605B
X	1.2599	2.1171	1.3450	1.2264	2.1893	2.6981
Y	1.2709	1.1422	1.1956	1.2209	1.0636	1.0239
R^2	0.9986	0.9836	0.9864	0.9942	0.9773	0.9784

Table 3
Mechanical properties of the test steels before the fatigue tests

Mechanical properties\steels	SS400	Acr-Ten A	1604A	1604B	1605A	1605B
YS (MPa)	325	395	431	473	545	551
UTS (MPa)	432	516	469	517	626	750
Elongation (%)	40.96	36.78	34.37	30.61	32.50	22.00

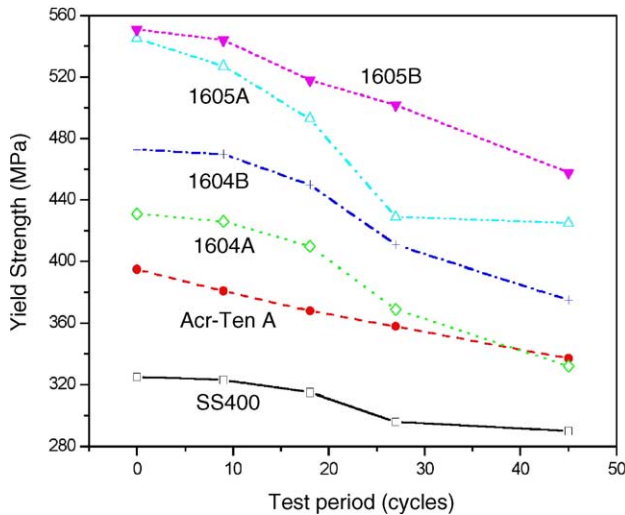


Fig. 5. Yield strength (YS) of the steels as a function of test cycles.

decrease in YS and UTS is the smallest for SS400. Interestingly, the YS and UTS for Acr-Ten A decrease quite linearly with an increase of the number of test cycles. On the other hand, the changes of the other four LAS are less regular, but decrease in general. These non-linear reductions in mechanical strength may be due to the negative effect of the surface roughness on the mechanical properties.

In Fig. 5, it is apparent that the yield strengths of 1604A, 1604B, 1605A, and 1605B are higher than those of Acr-Ten A and SS400. Furthermore, the YS of 1605A and 1605B are higher than 1604A and 1604B. The strengthening effects are due to the addition of manganese (1604A/B and 1605A/B) and chromium (1605A/B). Manganese will combine with sulfur to form globular MnS and it also strengthens the ferrite in steels by solid-solution strengthening. On the other hand, chromium will combine with carbon in steel to form carbides and also strengthen the steels. Because 1605A

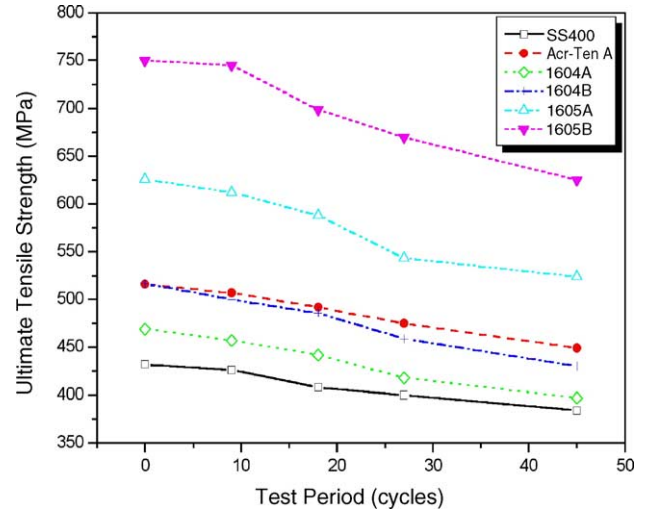


Fig. 6. Ultimate tensile strength (UTS) of the steels as a function of test cycles.

and 1605B contain both Cr and Mn, they have higher mechanical strength than the other test steels.

The changes in mechanical strength, while near linear, are scattered and insufficient data were accumulated to determine linear regression curves, such as $S = X \times t^Y$, that express the variation in strength with the number of test cycles [26], similar to Fig. 4. Therefore, we compared the mechanical strength and the weight loss for each steel after 45 cycles, as shown in Table 4. It is apparent that the reduction in the mechanical strength, especially of the yield strength, is greater than that of the cross-sectional area. Only the mechanical strength (YS and UTS) ratios for SS400 approach the value of remaining cross-section ratio. This may be attributed to the fact that the loosely adhering rust layers on the substrate of SS400 provide no local protection, so almost uniform corrosion occurred on the substrate thereby maintaining a smooth surface.

Table 4
Comparisons of mechanical strength, weight loss, and remaining cross-section after 45 cycles of accelerated corrosion tests

Steel	SS400	Acr-Ten A	1604A	1604B	1605A	1605B
Weight loss (mg/cm ²)	165.4	187.3	132.4	132.8	147	153.8
Thickness loss (μm) ^a	420.8	476.6	336.9	337.9	374	391.3
Remaining cross-section ratio ^b	0.905	0.908	0.899	0.901	0.901	0.893
Yield strength ratio ^c	0.892	0.853	0.770	0.793	0.780	0.831
Ultimate tensile strength ratio ^d	0.889	0.870	0.846	0.832	0.837	0.833

^a Thickness loss = weight loss / [(upper and lower surfaces) × (iron density)] = $\Delta w / 2A\rho$.

^b Remaining cross-section ratio = weight of the specimen (after the rust is stripped off) / weight of the specimen (without corrosion) (assuming the length of a specimen is not changed by corrosion).

^c Yield strength ratio = YS (45 cycles) / YS (0 cycle) [YS (0 cycle) is the mechanical strengths of an original (un-corroded) specimen].

^d Ultimate tensile strength ratio = UTS (45 cycles) / UTS (0 cycle) [UTS (0 cycle) is the mechanical strengths of an original (un-corroded) specimen].

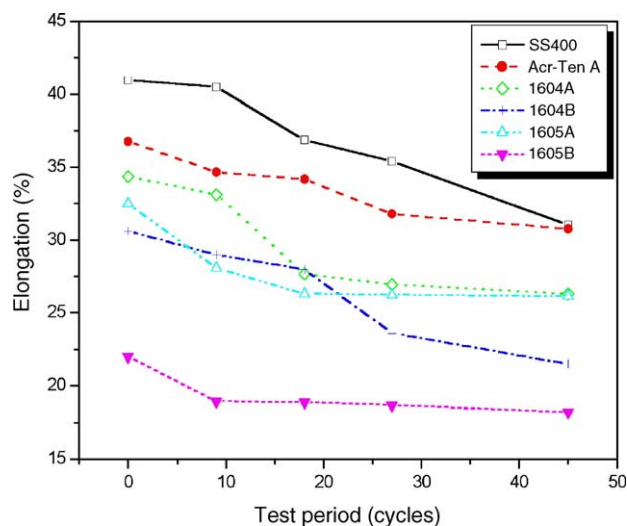


Fig. 7. Elongation (%) of the steels as a function of test cycles.

The smoother surface of SS400 after 45 cycles provided less chance of stress concentration than the rougher surfaces developed on the other alloys. The larger decrease in the YS and UTS for the latter alloys may also be due to localized corrosion such as pitting.

Fig. 7 illustrates the relationship between elongation and test period. It shows that elongation decreases with an increase in the number of test cycles, but that decreases are not linear. However, after 20 cycles, the elongations of 1605A and 1605B are not changed much. In addition, the ductility of the alloys are roughly 70–82% of their original values.

3.3. Analysis of the rust layers

The cross-sections of each steel after 18 and after 45 cycles of accelerated tests were observed by SEM, as shown in Fig. 8(a)–(h). It shows that the rust layers in these test steels all contain voids and/or micro-cracks, which facilitate the penetration of the chloride solution to the substrate, which, in turn, promotes the corrosion process. Most of the rust layers on the test steels were composed of two parts: the loose outer rust layer and the dense inner rust layer. After 18 cycles, the corrosion resistances of 1604A and 1604B are better than that of SS400, because the rust layers are denser and the voids and micro-cracks are fewer. The rust products on the two LAS (1604A/B) are similar to SS400—in that they can be removed easily from the substrate. The thickness of the rust layers on 1604A and 1604B after 18 test cycles are 100–200 μm thinner than that on SS400 ($\sim 400 \mu\text{m}$). On the other hand, the corrosion resistances of 1605A, 1605B, and Acr-Ten A are inferior to SS400 after 18 cycles. This is probably due to the fact that the drying time was not long enough in the cases of the adherent, dense, and deep-colored inner rust layers of the three LAS, thereby exposing the substrates of these steels to humid condition for longer periods of time, and allowing more corrosion. The superior corrosion resistance of SS400

at this stage (18 cycles) is caused by the gap (separation) between the rust layer and the substrate (Fig. 8(a)). This loose rust layer can easily be removed leaving the substrate basically untouched in a dry condition. In addition, it is difficult to transport chloride across the gap between the rust layer and the substrate. For those two reasons, the corrosion weight loss of SS400 was lower after longer test cycles (18–45 cycles).

After the accelerated tests were finished (72 cycles), the rust layers of SS400 were still easily removed and contained numerous voids. However, although most of the rust layer separated from the substrates of 1604A and of 1604B, parts of each rust layer did adhere, allowing localized corrosion, which made the substrate rougher than that of SS400. Furthermore, there were deep-colored inner rust layers found at the rust-layer/substrate interfaces of 1605A, 1605B, and Acr-Ten A. This indicates that the rust layers of these three LASs gradually form the thick (400–500 μm) and dense inner rust layers during the later cycles of the test. Experience with the stripping process and SEM observations suggested that the degree of difficulty in removing rust layers is dependent on the amount of chromium in the steels. The rust layers on the low-alloy steels with high-chromium content, such as 1605A, 1605B, and Acr-Ten A, are more compact and more difficult to remove. The dense, crack-free rust layers on Acr-Ten A and 1605A after 45 cycles are shown in Fig. 8(d) and (h), respectively.

3.4. Composition and structure of the rust

The composition of the rust layers after 18 cycles and after 45 cycles was analyzed using FTIR. The outer rust layers of each steel were quite similar after 18 and 45 cycles, and were composed of $\alpha\text{-FeOOH}$, $\gamma\text{-FeOOH}$, magnetite (Fe_3O_4), H_2O , and amorphous ferric oxyhydroxide ($\text{FeO}_x(\text{OH})_{3-2x}$, $x = 0$ to 1), as shown in Fig. 9(a) and (d). After stripping off the outer rust layers, the inner rust layers were analyzed, which showed that the main absorption peak for $\gamma\text{-FeOOH}$ became weaker (Fig. 9(b) and (e)). For Acr-Ten A, 1605A, and 1605B, almost no $\gamma\text{-FeOOH}$ was found in the surface rust layer (Fig. 9(c)). The surface rust layer means that the rust layer just covers above the substrate ($\sim 50 \mu\text{m}$ thick), and the inner rust layer is just under the outer rust layer.

These observations can be explained by acknowledging that the $\gamma\text{-FeOOH}$ was transformed into other kinds of corrosion products; for example, much of the $\gamma\text{-FeOOH}$ on WS was transformed into $\alpha\text{-FeOOH}$ after 45 cycles of the exposure in the experiment. Misawa et al. proposed that dissolved chromium and phosphorus ions enhance the formation of uniform amorphous ferric oxyhydroxide, which protects the steel substrate, and that this amorphous ferric oxyhydroxide will further transform into the more stable and protective structure of $\alpha\text{-FeOOH}$ [27,28]. However, the presence of Cl^- would lead to facile metal dissolution ($\text{Fe} \rightarrow \text{Fe}^{2+} + 2\text{e}^-$) by depassivating the iron surface. The acidic nature of the hydrated Fe^{2+} cation dissociates and therefore lowers the local pH via

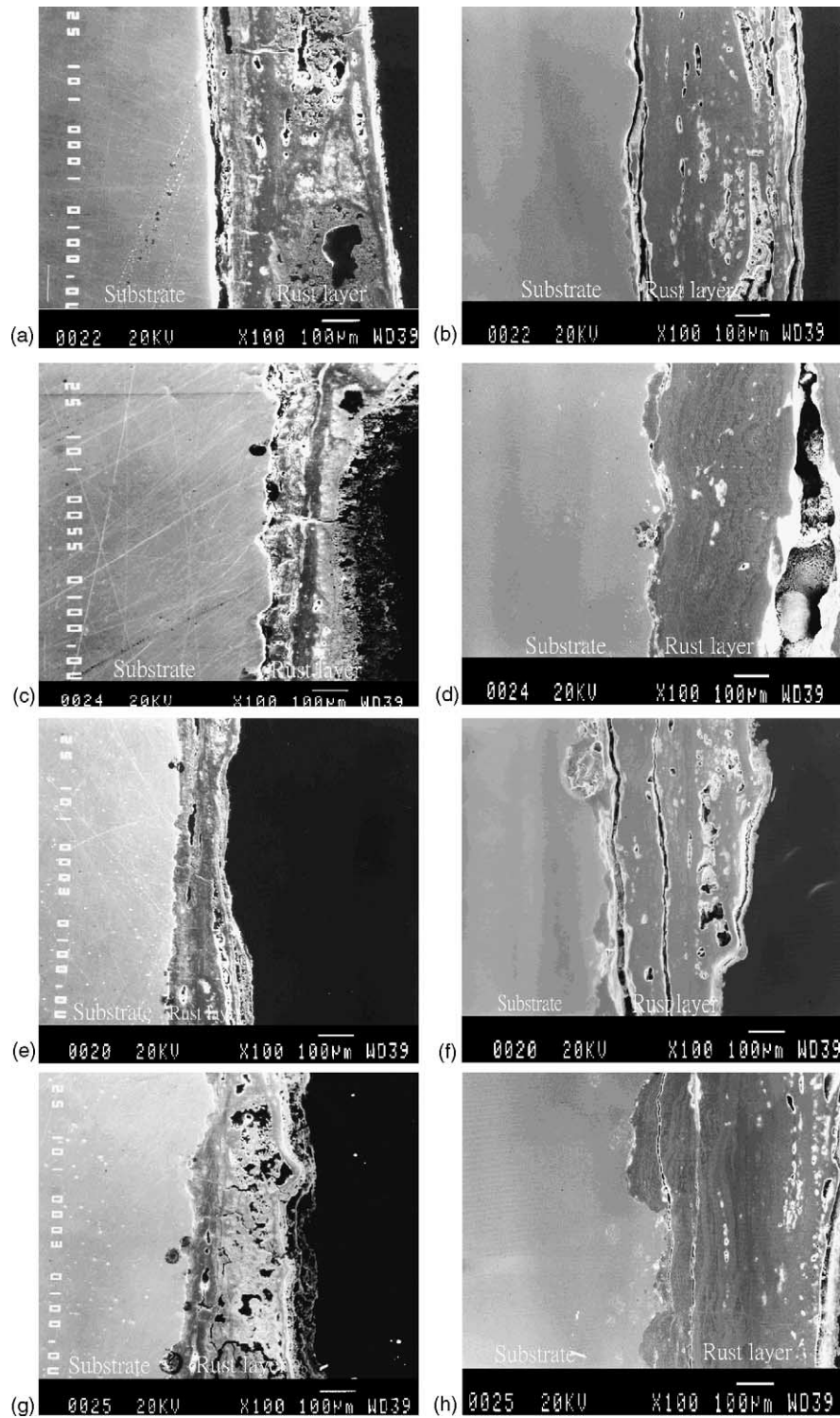


Fig. 8. Rust layers on the tested steel samples after 18 and 45 cycles of the accelerated corrosion tests: (a) SS400 (18 cycles), (b) SS400 (45 cycles), (c) Acr-Ten A (18 cycles), (d) Acr-Ten A (45 cycles), (e) 1604A (18 cycles), (f) 1604A (45 cycles), (g) 1605A (18 cycles), and (h) 1605A (45 cycles).

the following reaction:



This may promote the phase transformation to amorphous ferric oxyhydroxide ($\text{FeO}_x(\text{OH})_{3-2x}$, $x=0$ to 1) and

α - FeOOH . After 45 cycles in the cyclic corrosion test, the compact rust layers on the substrate of 1605A, 1605B, and Acr-Ten A were composed largely of Fe_3O_4 with a little of α - FeOOH (Fig. 9(c)). The valence of Fe in Fe_3O_4 is 8/3, which indicates that the dense rust layers prevent the dif-

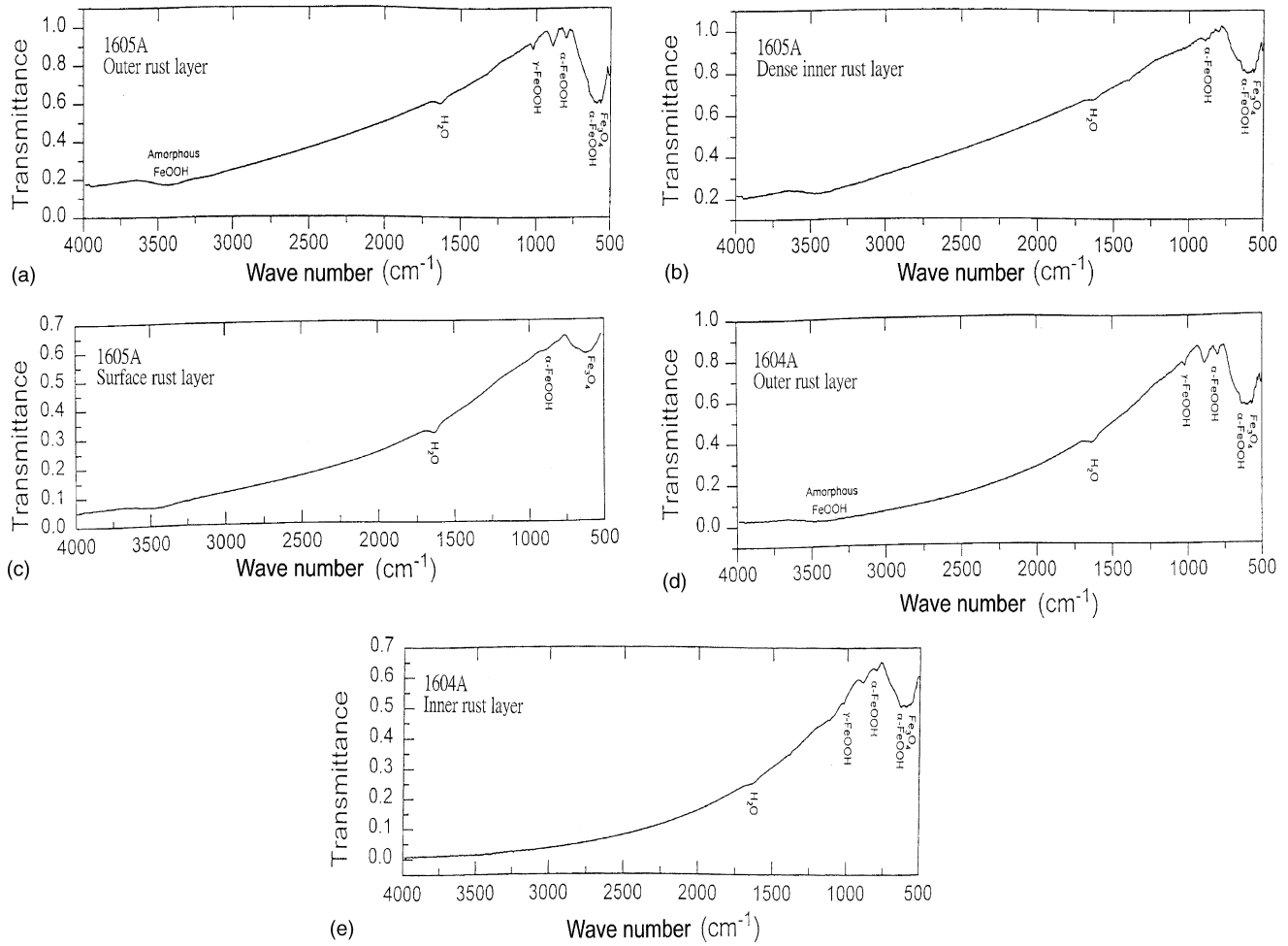
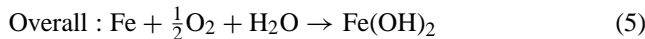
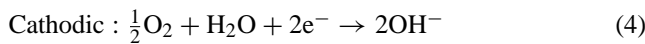


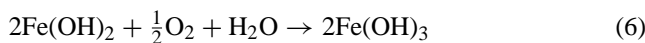
Fig. 9. FTIR spectra of the rust layers of the tested steels: (a) 1605A (outer layer), (b) 1605A (dense inner layer), (c) 1605A (surface layer), (d) 1604A (outer layer) and (e) 1604A (inner layer).

fusion of oxygen and result in the incomplete oxidation of Fe.

Rust forms on steel in air, which in the case of plain carbon steel does not provide protection, whereas it does on weathering steel, so the rusting rate tends to decrease [29,30]. In water containing dissolved oxygen, the following anodic and cathodic reactions occur:



Rust is formed by the further oxidation of Fe(OH)_2 with water:



Some researchers have drawn conclusions about the corrosion mechanisms from the rust compositions. For instance, some work indicates that $\gamma\text{-FeOOH}$ forms first and is then transformed to $\alpha\text{-FeOOH}$ and Fe_3O_4 [31–33]. Rust becomes rich in Fe_3O_4 but low in $\gamma\text{-FeOOH}$ in

coastal regions whereas rust formed in inland regions is rich in $\alpha\text{-FeOOH}$. On the other hand, Evans [34] assumed that the dissolution of iron ($\text{Fe} \rightarrow \text{Fe}^{2+} + 2e^{-}$) occurs at the substrate- Fe_3O_4 interface and that a cathodic reaction ($6\text{FeOOH} + 2e^{-} \rightarrow 2\text{Fe}_3\text{O}_4 + 2\text{H}_2\text{O} + 2\text{OH}^{-}$) occurs at the $\text{Fe}_3\text{O}_4/\text{FeOOH}$ interface. It was assumed that the reaction $\text{Fe}^{3+} \rightarrow \text{Fe}^{2+}$ occurs in the rust.

It must be noted that none of the FTIR examinations demonstrated the existence of $\beta\text{-FeOOH}$. This may be explained by the fact that the absorption band of $\beta\text{-FeOOH}$ is wide and is affected by the absorption bands of other ferric oxides and hydroxides due to the smaller quantity of $\beta\text{-FeOOH}$. Therefore, the absorption band of $\beta\text{-FeOOH}$ cannot be observed. In addition, Misawa et al. [27] proposed that an inner cohesive protective rust film is formed on low-alloy steels after long-term atmospheric exposure (industrial or urban). The protective film consists of amorphous $\delta\text{-FeOOH}$, the formation of which is catalyzed by copper and phosphorus of the steel surface; alternate drying and wetting favors development of its protective qualities. Keiser et al. [35] confirmed that the typical inner adherent rust layer consists mostly of $\delta\text{-FeOOH}$. However, it was not possible to determine whether

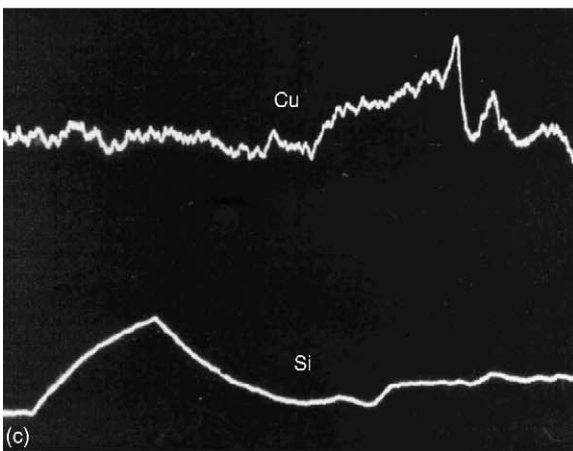
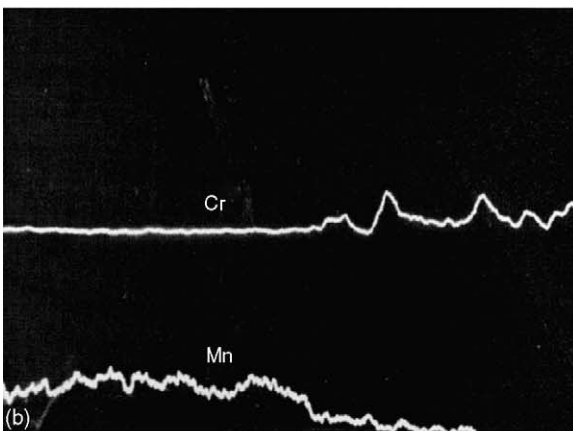
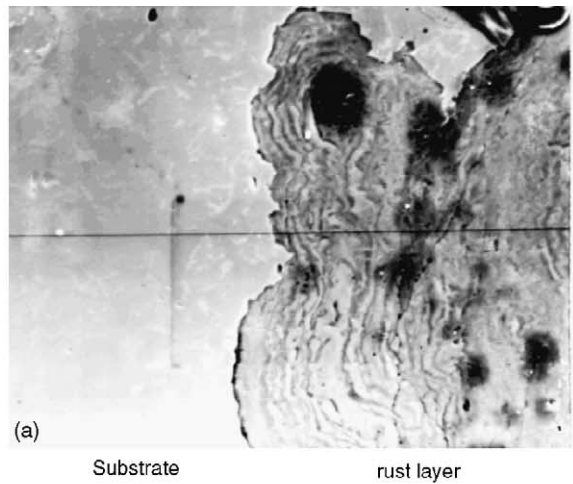


Fig. 10. EPMA line profiles of the rust layer/substrate for Acr-Ten A: (a) SEM photograph, (b) Cr and Mn, (c) Cu and Si.

δ -FeOOH existed or not in this study because the absorption band of δ -FeOOH is similar to that of amorphous ferric oxyhydroxide.

Examination of the cross-sections of the rust layers by EPMA showed the distributions of alloying elements for Acr-Ten A (Fig. 10) and 1605A (Fig. 11). The rust layer in Acr-Ten A was enriched in chromium but contained no manganese, as shown in Fig. 10(b). Furthermore, the interface was not

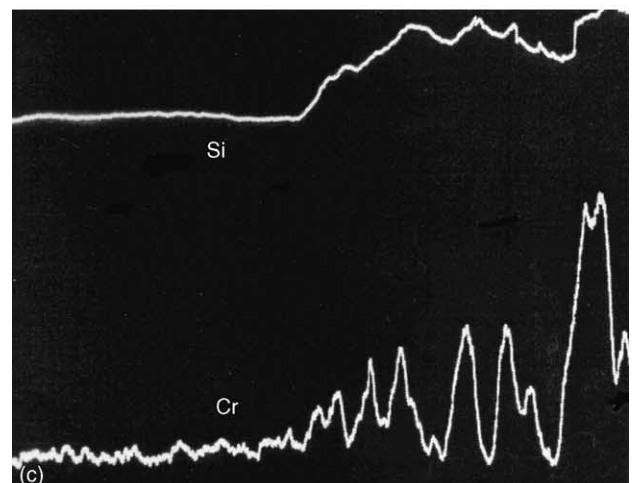
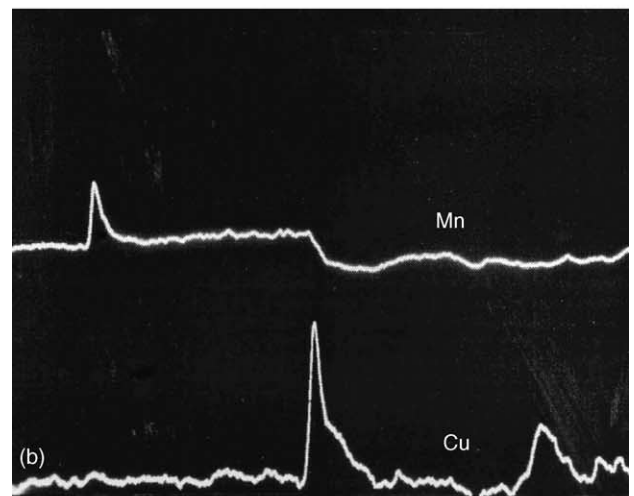
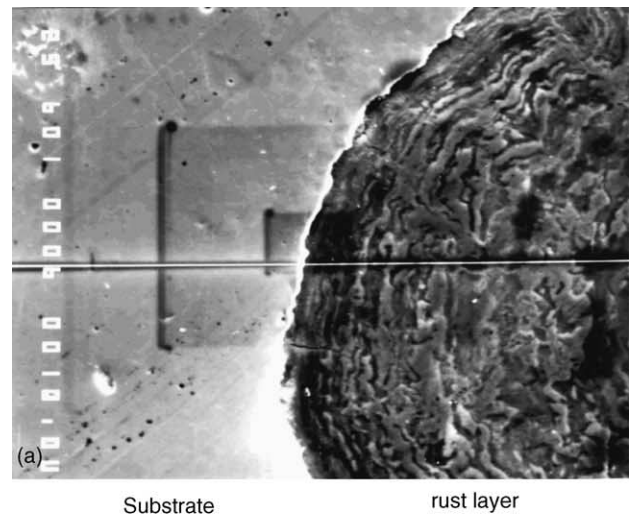


Fig. 11. EPMA line profiles of the rust layer/substrate for 1605A: (a) SEM photograph, (b) Cu and Mn, (c) Cr and Si.

obviously enriched in copper but copper was concentrated in the rust layer near the interface (Fig. 10(c)). In addition, the substrate was rich in silicon. On the other hand, the distributions of alloying elements in the rust are roughly the same

for 1605A and 1605B. Chromium and silicon were abundant in the inner rust layer of 1605A and 1605B after 45 cycles under the experimental conditions, as shown in Fig. 11(c). By contrast, copper concentrated at the interface between the rust layer and the substrate, while manganese decreased markedly from the interface to the rust layer, and seemed to disappear completely in the rust layer, as shown in Fig. 11(b).

In the research on weathering steels, several methods for increasing the corrosion resistance are described. For instance, one way is to alloy the steel with elements such as chromium, copper, and phosphorus, which enhance the densification and adhesion of the rust layers leading to better protection against corrosion. Another method is to lower the carbon content of the steels in order to reduce the strain energy and the amount of Fe_3C produced thereby increasing the corrosion resistance of the steel [7,17]. Alternatively, the addition of titanium combined with some substitutional elements, like carbon and nitrogen, can achieve the effect of lowering the strain energy of weathering steels [36].

As indicated above, chromium in WS plays an important role in enhancing the compactness, densification, and adhesion of the rust layers, thereby decreasing the diffusion of oxygen to the substrate. Furthermore, chromium can reduce the conductivity of the rust layers [37]. From the present EPMA analyses, it was found that chromium was gradually enriched in the rust layers (Fig. 11(c)), and that the dark regions in the rust layers were enriched with chromium while the light regions were chromium-depleted, as shown in Fig. 11(a). Under the severe wet/dry cyclic conditions in the present experiment, the Cr-rich dark inner rust layers were formed incompletely. As a result of the poor protection by the rust layers, serious corrosion of the substrate occurred.

Copper alloying additions may segregate during the dissolution of iron, and may adsorb on the surface of the steel [37–39]. On the other hand, copper will promote rust formation in the early stage of exposure, then will enrich the rust layers resulting in beneficial effects similar to those of chromium, i.e. of enhancing the protection and densification of the rust layers. In the present study, copper only concentrated obviously at the interface, which had little effect in promoting the protectiveness of the rust layers.

In addition, it is generally believed that manganese has no significant contribution in enhancing the weathering resistance of WS because of the absence of manganese in the rust layers, and that silicon should help to increase the corrosion resistance [26]. This can be confirmed by the fact that silicon was rich in the rust layers of both 1605A and 1605B, as shown in Fig. 11(c). However, the amount of silicon in the rust layer of Acr-Ten A was low (Fig. 10(c)). It is therefore concluded that silicon alloying additions may be helpful to enhance the protection and densification of the rust layers for 1605A and 1605B, and therefore their corrosion resistance is better than that of the common used WS (Acr-Ten A) even

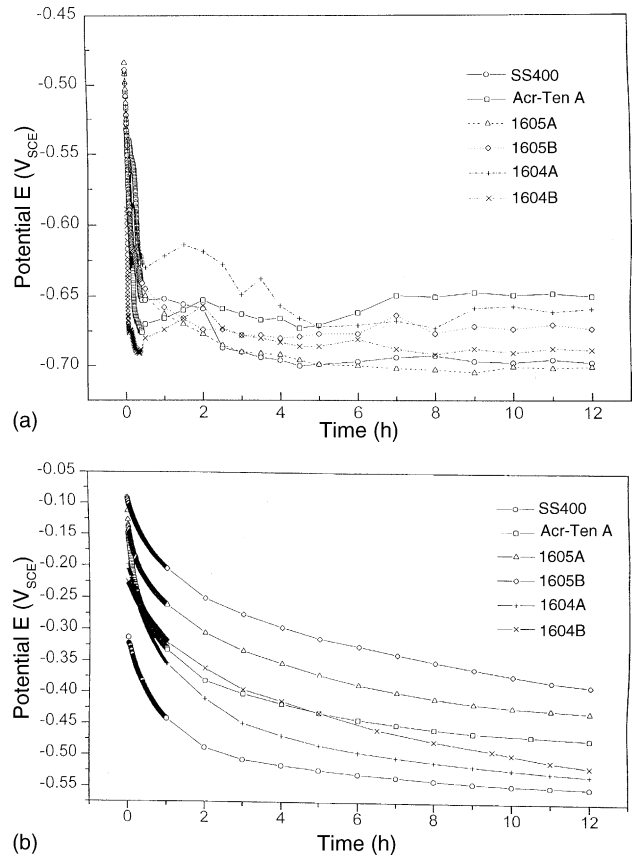


Fig. 12. Distribution of the corrosion potentials of the test steels immersed in 3.5 wt.% NaCl solutions at 25 °C: (a) before the accelerated corrosion tests, and (b) after the accelerated corrosion tests.

the C, Cu and Cr compositions (which appear to be most influential in determining corrosion resistance) of Acr-Ten A are almost identical to 1605A/B.

3.5. Corrosion potential measurements

Fig. 12(a) and (b), respectively illustrate the time dependence of the open-circuit potential, i.e. corrosion potential, for various steels during the immersion tests before (0 cycle) and after (72 cycles) the accelerated corrosion tests. The combination of the corrosion potential and the potential–pH diagram of a metal enable us to find out directly whether effective cathodic protection of the substrate is possible or not. The corrosion potential of Acr-Ten A was the noblest, and those of 1605A and SS400 were the most active among the six LASs during the 12 h immersion before the accelerated corrosion test. After prolonged immersion, all of the corrosion potentials dropped due to the dissolution of the corrosion products. The nobler corrosion potential of Acr-Ten A is believed to have resulted from the numerous rust-filled pores that developed after a longer immersion time, as shown in Fig. 13. On the other hand, the initial variations in corrosion potential for 1604A and 1604B were probably caused by the barrier effect of corrosion products [13]. The corrosion

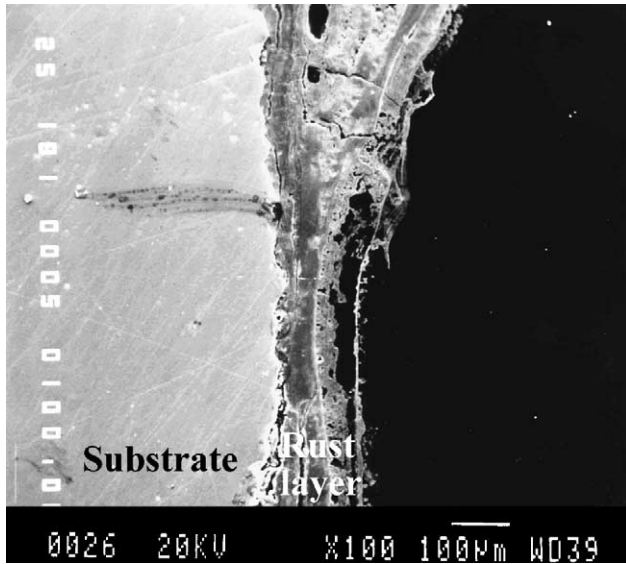


Fig. 13. Rust layers formed on Acr-Ten A after 12 h of immersion in 3.5 wt.% NaCl.

potentials of the test steels tended to be stable and unchanged with increasing immersion time. This is consistent with the presence of stable and protective rust layers formed on the surfaces of the steels. This rust may provide a barrier to the anodic reaction and consequently the dissolution of iron is mitigated.

In contrast, the corrosion potentials of the test steels all increased significantly after 72 cycles of accelerated corrosion tests. For instance, the corrosion potential of Acr-Ten A after immersion for 10 h in 3.5 wt.% NaCl increased from $-0.65V_{SCE}$ before the accelerated corrosion test to $-0.47V_{SCE}$ after the test. At this point in time, the corrosion potential of 1605B was the highest; that of 1605A was second, and the corrosion potential of SS400 was the most active. Steels can be ranked in order of decreasing corrosion tendency by listing them in order of increasing corrosion potential in 3.5 wt.% NaCl after 72 cycles of accelerated corrosion tests, as follows: SS400 > 1604A > 1604B > Acr-Ten A > 1605A > 1605B. The increase in the corrosion potential here is believed to be associated with an increase of the rust layer resistance. The higher the rust layer resistance, the nobler is the corrosion potential and the higher is the corrosion resistance of the steel. In addition, chromium within low-alloy steel decreases the conductivity of the rust layer and consequently leads to a rise in the corrosion potential [37]. It is worth noting that the corrosion potential of Acr-Ten A intersected that of 1604B at an immersion time of 5 h (Fig. 12(b)). After this immersion time, the corrosion potential of Acr-Ten A was nobler than that of 1604B. This may be explained by the fact that the outer rust layer of Acr-Ten A, formed after long-term atmospheric exposure (e.g., 45 cycles of accelerated tests), contained numerous pores that were subsequently filled with corrosion products formed in the chloride solution during the first 5 h of immersion. These corrosion products

sealed the pores and depressed the anodic reaction and therefore resulted in a nobler corrosion potential in the later stages of immersion.

In comparison with the corrosion potentials recorded before the accelerated corrosion tests, the variability of the corrosion potentials after the accelerated corrosion tests was significantly reduced. This can be explained by the presence of stable and protective rust layers formed on the steels' surfaces after long-term atmospheric exposure. Therefore, chloride cannot easily penetrate to the substrate to induce pitting corrosion or affect interfacial electric conductivity. On the other hand, the corrosion potentials of 1605A and 1605B after 72 cycles of testing increased significantly, and are even nobler than those of Acr-Ten A, which exhibited the noblest corrosion potentials prior to the accelerated corrosion tests. This is consistent with the concept that steels containing higher chromium and silicon, such as 1605A and 1605B, need a longer exposure time to reveal their corrosion resistance. According to previous results in this study, the corrosion rates of 1605A and 1605B in accelerated tests decreased markedly after ~ 30 cycles. This means that, under these severe cyclic wet/dry test conditions, a longer time was necessary to form adhesive dense rust layers on high-chromium steels, e.g. 1605A, 1605B. A similar phenomenon was observed for Acr-Ten A, but its weathering resistance was less significant than that of 1605A and 1605B.

Finally, the results of the accelerated tests indicate that the corrosion rates tend to decrease with an increase in the number of test cycles for 1605A and 1605B, similar to the behavior of Acr-Ten A. In addition, the mechanical strength of 1605A and 1605B are maintained after long periods of intermittent wet/dry corrosion testing. Furthermore, the rust layers on the two low-alloy steels have protective inner rust layer like Acr-Ten A. And the corrosion potentials of the two low-alloy steels are higher than other test steels after the accelerated corrosion tests showing lower corrosion tendencies. Therefore, it may be concluded that 1605A and 1605B are weathering steels seem to be more suitable for use in the humid and salty weather than Acr-Ten A.

4. Conclusions

1. The results of the chloride cyclic corrosion tests indicated that the susceptibility of the steels to corrosion can be listed in the following order based on their weight loss (from high to low): SS400 (pearlite/ferrite) > Acr-Ten A (pearlite/ferrite) > 1604B (ferrite) \geq 1604A (ferrite) > 1605B (bainite/ferrite) \geq 1605A (pearlite/ferrite).
2. The rust layers of LAS with high chromium content (1605A/B) were denser and could therefore provide better protection after longer periods of wet/dry cyclic corrosion. On the other hand, LASs with ultra-low carbon content (1604A/B) have even lower corrosion rates at earlier stages of accelerated corrosion.

3. The mechanical properties of the steels were degraded by corrosion partly because of the reduction in cross-section and partly because of the increase in surface roughness. The degree of degradation was least for SS400.
4. The copper and chromium additions to each steel can enrich the rust-layer/substrate interface and the rust layers, respectively. They can therefore enhance the compactness and densification of these rust layers. In chloride-containing environments, chromium should create a better densification of the rust layers.
5. The reason that corrosion potentials of the test steels are higher after the accelerated corrosion tests is because stable and protective rust layers had formed on the surface of the steels after the long-term atmospheric exposure.
6. The steels were ranked in order of decreasing corrosion tendency by listing them in order of increasing corrosion potential in 3.5 wt.% NaCl solution after 72 cycles of accelerated corrosion tests, as follows: SS400 > 1604A > 1604B > Acr-Ten A > 1605A > 1605B. The nobler corrosion potentials of 1605A and 1605B are consistent with the observation that the two LASs require a longer time to reveal their corrosion resistance.
7. Combining the results of the accelerated tests and the rust layer analysis, low-alloy steels such as 1605A and 1605B seem to be more suitable for use in the humid and salty weather than Acr-Ten A.

References

- [1] H. Okada, Y. Hosoi, H. Naito, *Corrosion* 26 (1970) 429.
- [2] B.R. De Meybaum, E.S. Ayllon, *Corrosion* 36 (1980) 345.
- [3] I. Suzuki, Y. Hisamatsu, N. Masuka, *J. Electrochem. Soc.* 127 (1980) 345.
- [4] H. Schmitter, H. Bohni, *J. Electrochem. Soc.* 127 (1980) 15.
- [5] M. Stratman, K. Bohnenkamp, T. Ramchandran, *Corros. Sci.* 27 (1987) 905.
- [6] T. Misawa, K. Asami, K. Hashimoto, S. Shimodaria, *Corros. Sci.* 14 (1974) 279.
- [7] H. Shirasawa, K. Mionoya, H. Tomari, T. Nakayama, *Kobelco Tech. Rev.* 12 (1991) 44.
- [8] J.C. Hudson, J.F. Stanners, *J. Iron Steel Inst., London* 180 (3) (1955) 271.
- [9] C.P. Larrabee, S.K. Coburn, in: L. Kenwoothy (Ed.), *Proceeding of the First Congress on Metallic Corrosion*, Butterworths, London, 1961, p. 276.
- [10] E. Williams, M. Komp, *Corrosion* 21 (1965) 9.
- [11] C. Southwell, A. Alexander, *Mater. Prot.* 9 (1970) 14.
- [12] J.H. Wang, L.I. Wei, H.C. Shih, *Corrosion* 52 (1996) 600.
- [13] J.H. Wang, L.I. Wei, H.C. Shih, *Corrosion* 52 (1996) 900.
- [14] T. Misawa, K. Hashimoto, S. Shimodaira, *Corros. Sci.* 14 (1974) 131.
- [15] M. Yamashita, T. Misawa, S.J. Oh, *Zairyo-to-Kankuo* 49 (2000) 82.
- [16] H.C. Shih, J.C. Oung, J.T. Hsu, J.Y. Wu, L.I. Wei, *Mater. Chem. Phys.* 37 (1994) 230.
- [17] H.H. Uhlig, *Corrosion and Corrosion Control*, third ed., Wiley and Sons, New York, 1991.
- [18] M. Pourbaix, A. Pourbaix, *Corrosion* 45 (1) (1989) 71.
- [19] ASTM E 8M-98, *Standard Test Methods for Tension Testing of Metallic Materials [Metric]*, 1998.
- [20] ASTM G 50-76, *Practice for Conducting Atmospheric Corrosion Tests on Metals* (West Conshohocken, PA: ASTM), 1992.
- [21] ASTM B 117-97, *Standard Practice for Operating Salt Spray (Fog) Apparatus*, 1997.
- [22] J. Davalos, M. Garcia, J.F. Macro, J.R. Gancedo, *Hyperfine Interact.* 69 (1991) 871.
- [23] ASTM G 1-88, *Standard Practice for Preparing, Cleaning, and Evaluating Corrosion Test Specimens*, 1988.
- [24] S. Feliu, M. Morcillo, *Corros. Sci.* 34 (3) (1993) 403.
- [25] R.A. Legault, A.G. Preban, *Corrosion* 31 (4) (1975) 117.
- [26] J. Kocich, *Corros. Sci.* 35 (1993) 1.
- [27] T. Misawa, T. Kyuno, W. Suetaka, S. Shimodaria, *Corros. Sci.* 11 (1971) 35.
- [28] K. Asami, M. Kikuchi, *Corros. Sci.* 45 (2003) 2671.
- [29] Y. Hisamatsu, *Boshoku Gijutsu (Corros. Eng.)* 20 (1971) 207.
- [30] T. Uno, S. Kado, *Bull. Jpn. Inst. Met.* 10 (1971) 208.
- [31] K.A. Chandler, J.E. Stanners, *Proceeding of the Second International Congress on Metallic Corrosion*, New York, NACE, Houston, Texas, 1963, p. 325.
- [32] J.E. Hiller, *Werkstoffe u Korrosion* 17 (1966) 943.
- [33] P. Keller, *Werkstoffe u Korrosion* 18 (1967) 865.
- [34] U.R. Evans, *Corros. Sci.* 9 (1969) 813.
- [35] J. Keiser, C. Brown, R. Heidersbach, *Corros. Sci.* 23 (1983) 251.
- [36] K.J. Irvine, T. Gladman, F.B. Pickering, *J. Iron Steel Inst.* 205 (1967) 161.
- [37] M. Yamashita, H. Miyuki, Y. Matsuda, H. Magano, T. Misawa, *Corros. Sci.* 36 (2) (1994) 283.
- [38] M. Stratmann, K. Bohnenkamp, T. Ramchandran, *Corros. Sci.* 27 (1987) 905.
- [39] Q.C. Zhang, J.S. Wu, J.J. Wang, W.L. Zheng, J.G. Chen, A.B. Li, *Mater. Chem. Phys.* 77 (2002) 603.